10-1-1999

Collisional Dynamics of Bi_2 $A(0_u^+)$. I. Quantum-resolved Vibrational Energy Transfer for v'=0–4

Robert E. Franklin
Air Force Institute of Technology

Glen P. Perram
Air Force Institute of Technology

Recommended Citation

Robert E. Franklin, Glen P. Perram; Collisional dynamics of Bi2 A(0+u). I. Quantum-resolved vibrational energy transfer for v'=0–4 . J. Chem. Phys. 1 October 1999; 111 (13): 5757–5763. https://doi.org/10.1063/1.479872

RESEARCH ARTICLE | OCTOBER 01 1999

Collisional dynamics of Bi_2 $A(0_u^+)$. I. Quantum-resolved vibrational energy transfer for $v'=0$–4

Robert E. Franklin; Glen P. Perram

J. Chem. Phys. 111, 5757–5763 (1999)
https://doi.org/10.1063/1.479872

Collisional dynamics of Bi_2 $A(0_u^+)$. I. Quantum-resolved vibrational energy transfer for $v'=0-4$

Robert E. Franklin[a] and Glen P. Perram[b]
Department of Engineering Physics, Air Force Institute of Technology, 2950 P Street, Wright-Patterson Air Force Base, Ohio 45433-7765

(Received 19 March 1999; accepted 9 July 1999)

Vibrational-to-translational energy transfer between the lowest vibrational levels ($v'=0-4$) of the $A(0_u^+)$ state of Bi_2 has been investigated using spectrally resolved, laser-induced fluorescence techniques. The small vibrational spacing ($\omega_e' \simeq 132\,\mathrm{cm}^{-1}$) leads to highly nonadiabatic conditions, particularly for the $Bi_2(A)$–He collision pair. However, the $\Delta v=-1$ transition probabilities for collisions with the rare gases range from 0.75% to 1.75% per collision, considerably lower than would be anticipated from standard vibrational energy transfer theory. Multiquantum ($\Delta v' = \pm 2$) transfer rates are low, consistent with the low anharmonicity of the $A(0_u^+)$ state. The rates for $\Delta v'=\pm 1$ transitions scale linearly with vibrational quantum number as expected near the bottom of this nearly harmonic potential. © *1999 American Institute of Physics.* [S0021-9606(99)01237-4]

I. INTRODUCTION

The $A(0_u^+)$ state of the bismuth dimer offers a unique opportunity to study quantum-resolved vibrational energy transfer under highly impulsive conditions. The vibrational frequency is low, $\omega_e' \simeq 132\,\mathrm{cm}^{-1}$, and the Bi_2–He collision involves a high relative speed at room temperature, yielding a ratio of collision time to the vibrational period of ~0.06. Theories which depend on perturbation approaches and adiabatic assumptions, such as the Schwartz, Slawsky, and Herzfeld (SSH) theory,[1] may overpredict the probability for energy transfer under these conditions.

While the spectroscopy of the Bi_2 $A(0_u^+)-X(0_g^+)$ system is reasonably well characterized,[2–4] very little is known about the collisional dynamics of $Bi_2(A)$. The radiative lifetime of $Bi_2(A)$ is 272–595 ns for $v'<20$, and a strong predissociation is observed near $v'=27$.[5,6] In the present study we examine the lowest vibrational levels, $v'=0-4$ to exclude the effects of predissociation. The rates for total collisional removal from a few (v',J') levels has been reported,[6] but no quantum-resolved vibrational or rotational transfer studies are found in the literature.

Several optically pumped $Bi_2(A-X)$ lasers were demonstrated in the late 1970s and early 1980s.[7,8] This laser operates at 590–790 nm with photon conversion efficiencies approaching 20%.[8] Bismuth dimers also play an important role in the NF($a\,^1\Delta$)–BiF($A0^+$) laser system.[9]

II. EXPERIMENT

The steady-state laser-induced flourescence apparatus is depicted in Fig. 1. A Coherent model 899-29 ring dye laser with Rhodamine 590 dye was used to selectively excite the $A(0_u^+)$ state via the $(v',v'')=(1,3)$, (2,4), (3,3), and (4,3) transitions near the maximum in the ground state rotational distributions, $J''=88-105$. Laser excitation spectra were recorded,[3,10] indicating the excitation of a pure (v',J') state. The dye laser was operated with a power of 0.3–0.9 mW and the laser linewidth was less than 100 MHz.

The bismuth dimer was generated by heating a small sample of granular bismuth (Mallinckrodt, 99.8%) in a 1 cm aluminum oxide crucible and tungsten basket heater to 900–1000 K. Such an apparatus typically produces about 33% atomic bismuth and 66% bismuth dimer.[6] The fluorescence cell consisted of a sixway (3.8 cm diam×20 cm length) stainless steel cross with quartz windows along the laser axis and for viewing the laser-induced fluorescence. The fluorescence cell could be evacuated to 8×10^{-6} Torr via an oil diffusion pump, and exhibited a room temperature leak rate of less than 3 mTorr/h. Typically, the cell was operated with 0.1–12.0 Torr of rare gases (99.996%) added to induce vibrational transfer. The rate of outgassing with the basket heater on was 1–2 mTorr/min. The cell pressure was monitored with MKS model 390 10 Torr and model 122A 100 Torr capacitance manometers.

The laser-induced fluorescence was resolved with a McPherson model 218 0.3 m monochromator with ~0.15 nm resolution. Spectra were recorded on a Princeton Instruments model 1024 S/RB optical multichannel analyzer (OMA). The signal was integrated for 1–4 mins to achieve a signal-to-noise ratio of ~150:1. A background spectrum was acquired prior to each laser-induced fluorescence spectrum by detuning the dye laser by ~0.03 cm^{-1}. The spectral response of the OMA was calibrated with a blackbody source at 1266 K.[10]

III. RESULTS

A. Spectrally resolved laser-induced fluorescence

A spectrum showing the effects of vibrational energy transfer after laser excitation of $v'=3$ is shown in Fig. 2.

[a]Present address: AFRL/DE, Kirtland Air Force Base, NM 87117-6008.
[b]Electronic mail: gperram@afit.af.mil

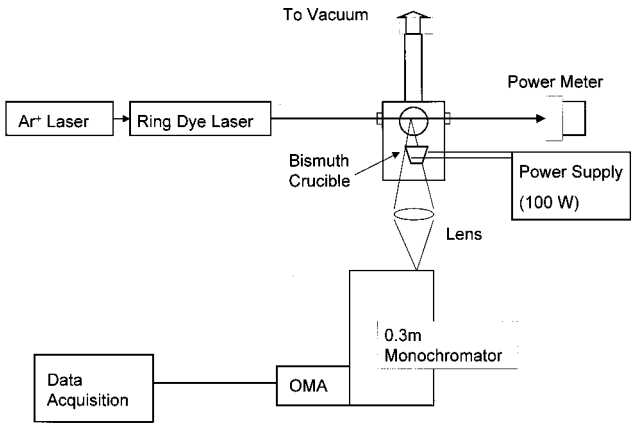

FIG. 1. cw spectrally resolved laser-induced fluorescence apparatus.

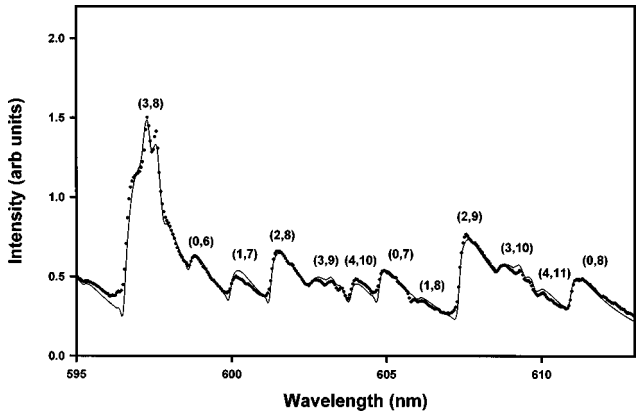

FIG. 2. $Bi_2(A-X)$ emission after laser excitation of ($v'=3$, $J'=87$) at $\nu = 17\,587.16\ cm^{-1}$ with 4.75 Torr of neon buffer gas: (○) observed spectrum, and (—) synthetic spectrum. Selected bandheads are labeled (v',v'').

Bandheads are labeled (v',v'') for some of the more prominent features. The spectrum was recorded for a neon buffer gas at 4.76 Torr and significant populations are observed in $v'=0-2$, indicating rapid vibrational energy transfer. The $P-R$ doublet emission from the laser excited $v'=3$, $J'=104$ level is evident in the (3,8) band. The $P-R$ doublet structure is not clearly evident in the other two bands originating from $v'=3$ due to low Franck–Condon factors. A spectral region with low Franck–Condon factors from the laser excited, or parent, state is desirable for quantifying the population in collisionally populated, or satellite states. Similar spectra were recorded for He, Ne, Ar, Kr, and Xe buffer gases at pressures of 0.1–12.0 Torr.

The spectrum of Fig. 2 is rather dense with significant overlap between vibrational bands. In order to determine the populations in various vibrational levels, synthetic spectra were fit to the observed spectra. Rather than specifying the emission from several thousand individual rotational lines, a basis function describing the general shape of the vibrational band was developed. Figure 3 illustrates the fit of such a basis function to the synthetically generated spectrum for the (3,3) emission band. The line positions and intensities for a thermal distribution of rotational levels for both the P and R branches of the (3,3) band are shown as lines of zero width across the bottom of Fig. 3. A convolution of these rotational features for a set of Gaussian lines of width 0.12 nm and a rotational temperature of $T=400$ K is also shown as the open circles (○) in Fig. 3. A double exponential function:

$$F(\lambda;a_v,b,c,\lambda_{vu})=\left(\frac{a_v b}{c-b}\right)\{\exp[-b(\lambda-\lambda_{vu})] - \exp[-c(\lambda-\lambda_{vu})]\}, \quad (1)$$

where a_v, b, and c are fit parameters and λ_{vu} represents the ($v'=v'$, $v''=u$) band origin, is an adequate basis function to represent the band shape. The area under the curve of Eq. (1) is conveniently the ratio of the a_v and c parameters, so that the population corresponding to vibrational level v is

$$N_v=a_v/c. \quad (2)$$

For bands characteristic of the Bi_2 A state, the integrated intensity from the basis function and the synthetic spectra agree within 2%.

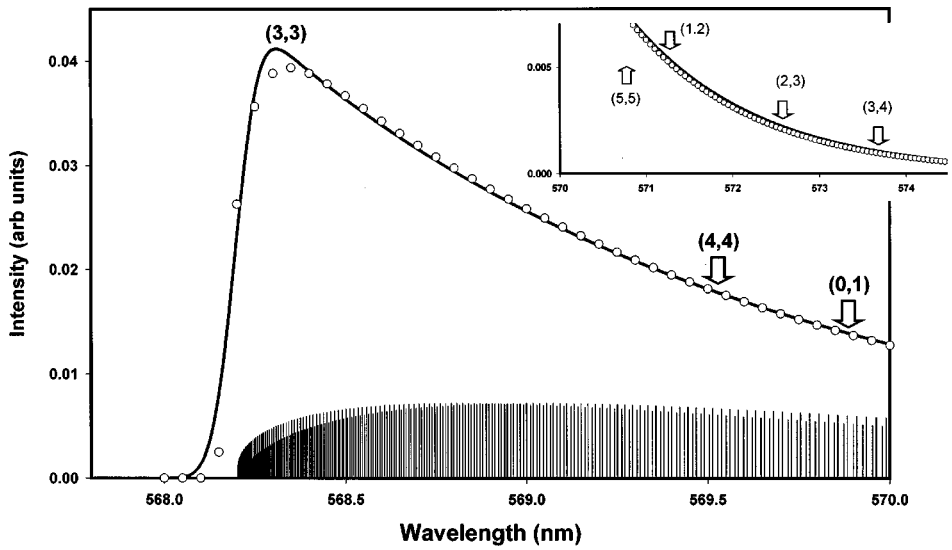

FIG. 3. A fit (—) of the double exponential basis function to a synthetic spectrum (○) of the isolated $Bi_2(A-X)$ (3,3) band for a rotational temperature of 400 K and a resolution of 0.12 nm. The inset is an extended view for high rotational levels indicating the location of adjacent bandheads labeled (v',v'').

This basis function is particularly good at predicting the band intensity for high rotational levels. As seen in Fig. 3, there are at least five bandheads from nearby transitions that overlap with emission from higher rotational levels of the (3,3) band. Thus, extrapolation to high J using this basis function is a critical feature in fitting the synthetic spectra to the observed emission. The intensity at high rotational levels is sensitive to the rotational temperature, which is strongly correlated with the fit parameter c. By fitting a series of synthetic spectra with differing rotational temperatures, this fit parameter is found to vary with temperature as $c=\alpha+\beta T^{\gamma}$ where $\alpha=0.0493\pm0.007$, $\beta=601\pm38$, and $\gamma=1.14\pm0.01$. The fit parameter, b, primarily affects the rise in intensity near the band origin, and is primarily determined by monochromator resolution.

In the parent vibrational level, the rotational distribution is nonthermal, due to the selective laser excitation of a single rotational level. To incorporate the P,R-doublet emission from laser excited state, two Gaussian lines, centered at $\lambda_0=\lambda_R$ and λ_p and of full width at half-maximum, $\Delta\lambda$, are added to the synthetic spectrum:

$$G(\lambda;A,\Delta v,\lambda_0)=\left(\frac{A\lambda^2}{c\Delta\lambda}\right)\left(\frac{4\ln 2}{\pi}\right)\times\exp\left[-4\ln 2\left(\frac{\lambda-\lambda^2/\lambda_0}{\Delta\lambda}\right)^2\right]S(J_0). \tag{3}$$

The rotational line strength,

$$S(J)=\begin{Bmatrix} J/(2J+1), & P \text{ branch},\\ (J+1)/(2J+1), & R \text{ branch}\end{Bmatrix}\cong 0.5 \text{ for large } J, \tag{4}$$

is modified by nuclear spin ($I=9/2$) statistics with a ratio of $R=(I+1)/I=1.22$.[11]

To model the spectrum observed in Fig. 2, a series of basis functions representing each observed vibrational band are summed. The resolution and rotational temperature are constant for a particular spectrum, and thus the fit parameters b and c are common for each collisionally populated vibrational band. The rotational temperature of the parent state is typically different than the satellite states, due to the effects of pure $R-T$ transfer versus V, $R-T$ transfer. Therefore, the synthetic spectrum is represented as

$$I(\lambda)=\sum_{v\neq v_0}\sum_u q_{vu}F(\lambda;a_v,b,c,\lambda_{v,w})+\delta_{v,v_0}\sum_w q_{vw}\begin{Bmatrix}F(\lambda;a_{v_0},b_0,c_0,\lambda_{v,w})\\ +G(\lambda;A,R,\lambda_P)+G(\lambda;A,R,\lambda_R)\end{Bmatrix}, \tag{5}$$

where

$q_{v,u}$ = Franck–Condon factor for the (v,u) emission band,

$$\delta_{v,v_0}=\begin{cases}1, v=v_0\\ 0, v\neq v_0,\end{cases}$$

where v_0 is the parent vibrational level.

A least-squares fit of Eq. (5) to the observed spectrum is shown in Fig. 2. Constraining the fits to the known Franck–Condon factors, band origins, $P-R$ doublet wavelengths, and monochromator resolution, yields the following fit parameters: a_v, b, c, b_0, c_0, and A. The resulting c and c_0 parameters correspond to rotational temperatures of 602 ± 85 and 248 ± 32 K for the satellite and parent states, respectively. The relative population in a satellite level to the parent level is then specified by the ratio of integrated intensities, or areas, as

$$\frac{N_v}{N_{v_0}}=\frac{a_v/c}{a_{v_0}/c_0+2A}. \tag{6}$$

The comparison between the observed and fit spectra, as shown in Fig. 2, is generally adequate. The differences are largely attributed to vibrational bands excluded from the spectral simulation.

B. Quantum-resolved vibrational transfer rates

The relative vibrational populations after laser excitation of $v'=3$ as a function of neon buffer gas pressure are shown in Fig. 4. The populations in $v'=4$, 2, and 1 increase linearly at low pressures, but exhibit curvature for pressures above a few Torr due to multiple collisions that remove population from the satellite state. The relative populations in the satellite levels $v'=2$ and 1 near 10 Torr is approximately 1.3, as compared to the equilibrium value of $N(v'=2)/N(v'=1)=\exp[-\omega_e/kT]\approx0.5$. Significant vibrational relaxation has occurred at 10 Torr buffer gas pressure, but the distribution is still far from equilibrium. The population in $v'=0$ exhibits curvature at low pressures, indicative of population cascading through intermediate vibrational levels.

In order to extract state-to-state vibrational transfer rate coefficients from data similar to that shown in Fig. 4, a steady-state analysis of the master rate equation is required. The master rate equation for the population in vibrational level v is:[12]

$$\frac{dN_v}{dt}=S\delta_{v,v_0}+\sum_w R_{vw}N_w, \tag{7}$$

where w is the quantum number for other vibrational levels of $Bi_2(A)$, S is the rate for laser excitation of the parent level v_0, and R_{vw} denotes the rate coefficient matrix:

$$R_{vw}=k_{VT}(w\rightarrow v)[M]-\delta_{vw}\left\{\Gamma_r+k_Q(v)[M]+\sum_w k_{VT}(v\rightarrow w)[M]\right\}. \tag{8}$$

The goal of this work was to extract the rate coefficients for vibrational transfer from state w to state v, $k_{VT}(w\rightarrow v)$, from the rate matrix, R_{vw}. The radiative decay rate for $Bi_2(A,v'\leqslant3)$ is $\Gamma_r=1.6-2.3\times10^6\ s^{-1}$.[6] The radiative rate has no systematic dependence on vibrational level and shortening of the collisionless decay rate due to predissociation does not

occur until vibrational levels near $v'=27$.[6] The rate coefficient for electronic quenching, k_Q, may depend on vibrational level and the total removal of population from the level v due to vibration transfer is represented by the summation, $\Sigma_w k_{VT}(v\rightarrow w)$.

For the cw laser source employed in the present work, the $Bi_2(A)$ system attains steady-state conditions, $dN_v/dt=0$, and Eq. (9) reduces to a linear system of algebraic equations:

$$\sum_w R_{vw}N_w = S\delta_{v,v_0}. \tag{9}$$

For a given rate matrix, R_{vw}, the relative populations can easily be determined as

$$\frac{N_v}{N_{v_0}} = \frac{k_{VT}(v_0\rightarrow v)[M]/\Gamma_r}{1+[k_Q(v)[M]+\Sigma_w k_{VT}(v\rightarrow w)][M]/\Gamma_r - \Sigma k_{VT}(w\rightarrow v)\left[\frac{N_w}{N_v}\right][M]/\Gamma_r}. \tag{10}$$

The third term in the denominator of Eq. (10) represents multiple collisions that populate the observed vibrational level. In general, this term possesses a complicated pressure dependence. However, at low pressures where multiple collisions are not significant, Eq. (10) reduces to the form

$$\frac{N_v}{N_{v_0}} = \frac{Ax}{1+Bx}, \tag{11}$$

where

$$A = k_{VT}(v)/\Gamma_r,$$

$$B = \left\{ k_Q(v) + \sum_w k_{VT}(v\rightarrow w) \right\} \Big/ \Gamma_r,$$

$$x = [M].$$

Equation (11) has often been successfully employed to determine the vibrational-to-translational ($V-T$) transfer rates.[12–14]

Figure 4 illustrates a least-squares fit of Eq. (11) to the data, providing an initial estimate of the state-to-state $V-T$ rate coefficients, as reported for neon in Table I. The data for $v'=0$ cannot be adequately represented by Eq. (11), since single collision transfer involving $\Delta v=-3$ is insignificant. Similar data were recorded for laser excited states $v'=1-4$ and for He, Ne, Ar, Kr, and Xe buffer gases.

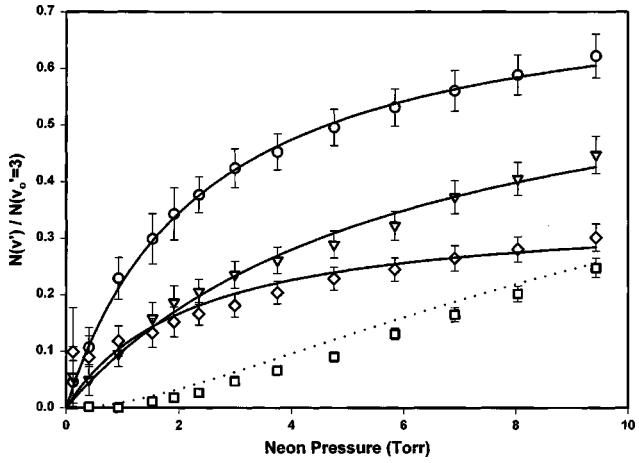

FIG. 4. Vibrational population distributions as a function of neon buffer gas pressure after laser excitation of $v'=3$. The observed populations for: (○) $v'=2$, (▽) $v'=1$, (◇) $v'=4$, and (□) $v'=0$ are fit to: (—) Eq. (11), and (---) the constrained rate matrix of Eq. (9).

In order to refine the determination of the vibrational transfer rate coefficients, the full rate matrix of Eq. (9) is utilized. To reduce the number of independent matrix elements, the following assumptions were applied. Detailed balancing is used to specify transitions that increase vibrational energy:

$$k_{VT}(v\rightarrow w) = k_{VT}(w\rightarrow v)\exp[-(E_w-E_v)/kT]. \tag{12}$$

Linear scaling of the vibrational transfer rate coefficients with vibrational quantum number as predicted for harmonic oscillators is applied.[15]

$$k_{VT}(v\rightarrow v-1) = vk_{VT}(1\rightarrow 0). \tag{13}$$

Transfer involving multiquanta is assumed to be a fixed fraction of the $\Delta v=-1$ rate:

$$k_{VT}(v\rightarrow v-2) = fk_{VT}(v\rightarrow v-1) \tag{14}$$

and the rates for $|\Delta v|\geqslant 3$ are neglected. The electronic quenching and radiative rates are assumed independent of vibrational level. With these assumptions and the initial estimates for the single collision rate coefficients, the full rate matrix, R_{vw}, is specified. By varying the quantities $k_{VT}(v\rightarrow v-1)$, k_q, and f, a single rate matrix which best represents the full set of spectrally resolved laser-induced fluorescence data can be established. The predicted population in $v'=0$ after laser excitation of $v'=3$ using this rate matrix approach is shown in Fig. 4. The corresponding predictions for $v'=4$, 2, and 1 are quite similar to the fits from Eq. (11). The resulting rate parameters for neon collisions are pro-

TABLE I. Vibrational transfer rate coefficients for neon (10^{-12} cm^3/molecule s).

v	$k_{VT}^{Ne}(v\rightarrow v-1)$ [from eq. (11)]	$k_{VT}^{Ne}(v\rightarrow v-1)$ (from rate matrix)	k_{eq}	f
1	6.3±0.7	6.2±0.7	<0.9	0.16
2	9.6±0.7	9.6±0.7	<2.9	0.10
3	15.1±1.4	14.1±1.4	<3.3	0.12
4	19.6±3.5	19.2±3.5	<3.3	0.05

TABLE II. Fundamental vibrational transfer rate coefficients for rare gases (10^{-12} cm^3/molecule s).

Buffer gas	Laser excited v'	$k_{VT}(v \rightarrow v-1)$	$k_{VT}(1 \rightarrow 0)$	$\sigma_v(1,0)/\sigma_g$
He	2	10.6±1.5	5.3±0.7	0.0075
Ne	1–4	(See Table 1)	4.8±0.9	0.0142
Ar	3	7.6±1.2	2.5±0.4	0.0089
Kr	2	4.8±0.7	2.4±0.4	0.0112
Xe	2	6.8±1.3	3.4±0.7	0.0175

vided in Table I. The total vibrational removal rate dominates the electronic quenching rate in determining the total rate for deactivation of a given vibrational level. Therefore, only an upper bound for the electronic quenching rates is reported. Note that the single collision analysis of Eq. (11) provides an adequate description for the vibrational levels adjacent to the laser excited state.

Collisions with the remaining rare gases were studied in somewhat less detail. The vibrational levels examined and resulting rate coefficients are reported in Table II.

IV. DISCUSSION

A. Comparison to previous studies

Collisionless lifetimes and total quenching rates have been examined previously using time-resolved laser-induced fluorescence techniques.[5,6] The cross section for total quenching of $Bi_2(A, v'=1, J'=10)$ has been reported as 56×10^{-16} cm^2 and at $T=300$ K,[6] and the corresponding rate coefficient is 2×10^{-10} cm^3/molecule s. This rate is several orders of magnitude greater than the vibrational transfer rates measured in the present work. The earlier studies focused on determining the collisionless decay rates and employed a monochromator to limit the fluorescence to a specific rotational level. Thus, the observed total quenching rates include both vibrational and rotational removal processes. The magnitude of these quenching rates is consistent with total rotational removal from the laser excited state.

While an early study of $Bi_2(A)$ photoluminescence spectra indicated collisionally populated (v,J) states,[16] no quantum-resolved vibrational or rotational energy transfer has previously been reported.

B. Validity of scaling relationships

The linear scaling of the $\Delta v=-1$ rate coefficients with vibrational quantum number as expressed by Eq. (13) is demonstrated for the lowest vibrational levels of $Bi_2(A)$ in Fig. 5. The rate for transfer from $v'=4$ to $v'=3$ is about 6% of the gas kinetic rate. A linear fit to the data provides a single best estimate for the fundamental vibrational transfer rate coefficient, $k_{VT}^{Ne}(1,0)=4.8\pm0.9\times10^{-12}$ cm^3/molecule s. The Landau–Teller scaling for harmonic oscillators is clearly adequate for describing $V-T$ transfer within the lowest vibrational levels of $Bi_2(A)$.

Figure 6 indicates a temperature of $T=200-300$ K is required for the observed vibrational transfer rates to obey the principal of detailed balancing, as expressed in Eq. (12). While the granular bismuth was heated to 900–1000 K in the tungsten basket heater, the Bi/Bi_2 vapor expands into the fluorescence chamber and condenses on the cell walls. The rotational temperature was independently determined from the intensities observed in rotationally resolved laser excitation spectra as 316±29 K.[3,10] Most of the data shown in Fig. 6 would be consistent with this rotational temperature.

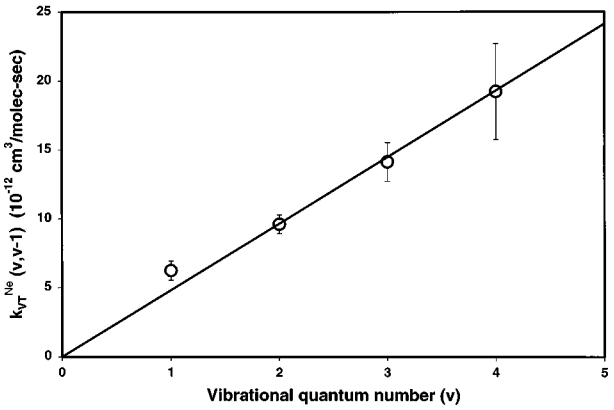

FIG. 5. Scaling of the $\Delta v=-1$ rate coefficients with neon as the buffer gas with vibrational quantum number indicates a linear trend, as predicted by the Landau–Teller model (Ref. 16).

The synthetic spectra discussed in Sec. III A also provides information regarding the rotational temperature of the observed fluorescence. The rotational temperature of the laser excited vibrational levels was 363±76 K, consistent with the temperatures discussed above. However, the temperature of the collisionally populated vibrational levels was 602 ±51 K. The rotational levels excited by the laser, $J_0=88-105$, were considerably higher than the rotational level where the maximum in the Boltzmann distribution occurs, $J_{max}=69$. These results suggest that collisions involving a change in both vibrational and rotational state do not completely thermalize the rotational distribution. Quantum-resolved rotational energy transfer in these low lying vibrational levels of $Bi_2(A)$ will be reported in a subsequent paper.

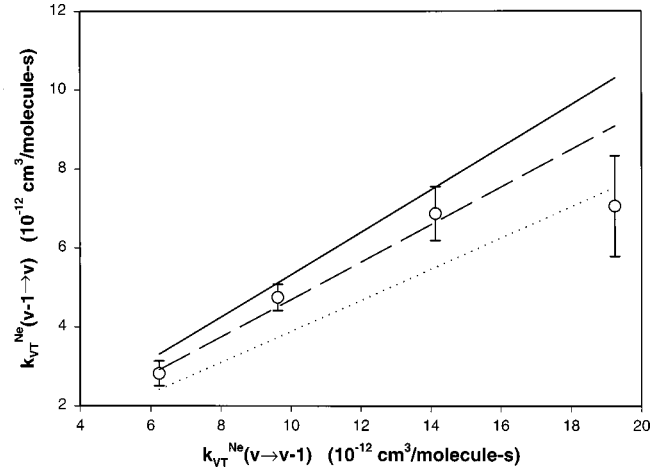

FIG. 6. Comparison of (○) observed $v \rightarrow v-1$ and $v-1 \rightarrow v$ rate coefficients for neon with the principle of detailed balancing for a temperature of:(···) 200 K, (---) 250 K, and (—) 300 K.

The rates for $\Delta v=-2$ are only 5%–16% of the corresponding $\Delta v=-1$ rates, as shown in Table II. Similar results have been observed for Br_2 $B\,^3\Pi(0_u^+)$.[17] However, the multiquantum fraction for BrCl $B\,^3\Pi(0^+)$ is considerably higher, $f=0.4$.[12] BrCl(B) is considerably more anharmonic than either $Br_2(B)$ or $Bi_2(A)$. These results are consistent with previous conclusions that the anharmonicity of the oscillator wave functions is more important than higher order terms in the interaction potential in determining the magnitude of multiquantum transfer.[18]

C. Impulsive collisions and the Schwartz, Slawsky, and Herzfeld theory

The Schwartz, Slawsky, and Herzfeld (SSH) theory[1] successfully predicts the probability for vibrational transfer ($V-T$), particularly the scaling with mass and vibrational frequency, under a wide range of conditions.[19] The SSH theory depends on the first-order Born approximation, models a harmonic oscillator perturbed by an exponential interaction potential, and assumes a relatively nonimpulsive, or near adiabatic, collision. The SSH theory predicts the probability for vibrational transfer as[19]

$$P(1,0)=\frac{\sigma(1,0)}{\sigma_g}=M\left(\frac{\Theta'}{\Theta}\right)\left(\frac{\Theta'}{T}\right)^{1/6}\times\exp\left[-3/2\left(\frac{\Theta'}{T}\right)^{1/3}+\left(\frac{\Theta}{2T}\right)+\left(\frac{\epsilon}{kT}\right)\right], \tag{15}$$

where

$$M=\sqrt{\frac{2\pi}{3}}\frac{2m_A^2m_Bm_C}{(m_B+m_C)(m_A+m_B)^2\mu},$$

$$\mu=\text{collision pair reduced mass}=\frac{m_A(m_B+m_C)}{m_A+m_B+m_C},$$

$$\Theta'=4\pi^2L^2(2\pi c\omega_e)^2\mu/kT,$$

$$\Theta=hc\omega_e/kT,$$

$\omega_e=$ fundamental vibrational frequency (cm^{-1}),

$\epsilon=$ potential well depth,

$L=$ potential interaction length,

$\sigma_g=$ gas kinetic or hard sphere cross section.

Surveying the existing database of $V-T$ transfer for the diatomic halogens indicates a deficiency of the SSH theory for highly impulsive collisions.[17] By converting the observed $V-T$ transfer rate coefficients to a transition probability, using the specified masses, vibrational frequency, and translational temperature, and assuming a small well depth, $\epsilon/kT\approx 0$, the interaction lengths, L, required to satisfy Eq. (15) are specified and displayed in Fig. 7. For adiaticity, $\xi=c\omega_eL/(\sqrt{8kT/\pi\mu})>0.3$, the interaction lengths are in the range $L=0.25-0.10$, which is typical for $V-T$ transfer.[19] However, the most impulsive collisions, particularly the $Bi_2(A)-He$ interaction, require unreasonably large interaction lengths. In other words, the SSH theory overpredicts the probability for $V-T$ transfer involving highly impulsive conditions. A large interaction length artificially reduces the prediction to generate agreement with the observed rates.

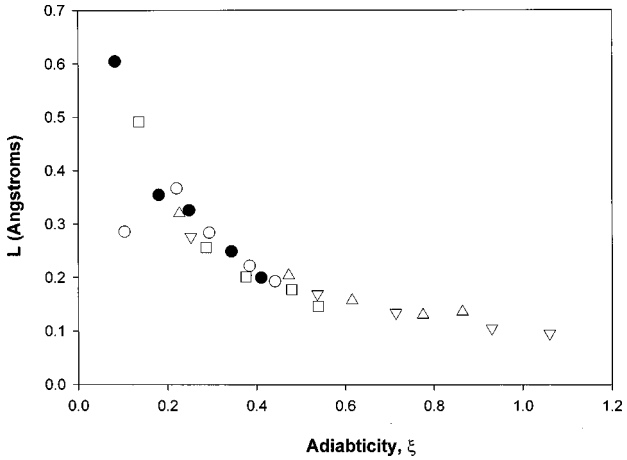

FIG. 7. The interaction length derived using the SSH theory of Eq. (15) from $V-T$ rate coefficients observed for: (●)$Bi_2(A)$ (present work), (○)$Br_2(B)$ (Ref. 18), (□)BrCl(B) (Ref. 13), (△)BrF(B) (Ref. 22), and (▽)IF(B) (Ref. 14). The adiabaticity is defined as the collision interaction time relative to the vibrational period, $\xi=c\omega_eL/(\sqrt{8kT/\pi\mu})$. To evaluate the adiabaticity, a constant value for the interaction length was chosen, $L=0.02$ nm.

There are several approximations made in the SSH theory that depend on near adiabatic conditions: (1) the first-order Born approximation is used to compute the transition probability, (2) the matrix elements for the exponential interaction potential are approximated by a first-order Taylor series, and (3) when averaging over the velocity distribution, the approximation $\text{csch}^2(2\pi^2c\omega_eL/v)\approx 4\exp(-4\pi^2c\omega_eL/v)$ is employed. The latter two approximations can be improved,[20,21] but the differences are not sufficiently large to account for the interaction lengths computed in Fig. 7. The large interaction lengths for the most impulsive collisions ($\xi<0.3$) appear to result from the failure of the first-order Born approximation.

V. CONCLUSION

Vibrational energy transfer in the lowest vibrational levels of $Bi_2(A)$ is rapid, although somewhat less than predicted by the SSH theory. The $Bi_2(A)$ potential is nearly harmonic, leading to a linear scaling of the vibrational transfer rates with vibrational quantum number and a low probability for multiquantum transfer. Interaction lengths for bismuth dimer–rare gas collisions are consistent with those derived for the diatomic halogens when the collision pair exhibits the same adiabaticity.

[1] R. N. Schwartz, Z. I. Slawsky, and K. F. Herzfeld, J. Chem. Phys. **20**, 1591 (1952).
[2] R. F. Barrow, F. Taher, J. D. Incani, C. Effantin, A. J. Ross, A. Topovzkhanian, G. Wannous, and J. Verges, Mol. Phys. **87**, 725 (1996).
[3] R. E. Franklin and G. P. Perram, J. Mol. Spectrosc. **194**, 1 (1999).
[4] G. Gerber, Honinger, and J. James, Chem. Phys. Lett. **85**, 415 (1982).
[5] J. M. Blondeau, G. Gandara, P. Carette, and J. Messelyn, Chem. Phys. Lett. **71**, 246 (1980).
[6] G. Ehret and G. Gerber, Chem. Phys. **66**, 27 (1982).
[7] W. P. West and H. P. Broida, Chem. Phys. Lett. **56**, 283 (1978).

[8] S. Drosch and G. Gerber, J. Chem. Phys. **77**, 123 (1982).
[9] D. J. Benard, J. Appl. Phys. **74**, 2900 (1993).
[10] R. E. Franklin, Ph.D. dissertation, Air Force Institute of Technology, AFIT/DS/ENP/97-04, 1997.
[11] G. Herzberg, *Molecular Spectra and Molecular Structure-I. Spectra of Diatomic Molecules* (Van Nostrand Reinhold, New York, 1950).
[12] G. P. Perram and S. J. Davis, J. Chem. Phys. **98**, 373 (1993).
[13] P. J. Wolf and S. J. Davis, J. Chem. Phys. **87**, 3492 (1987).
[14] R. B. Kurzel and J. I. Steinfeld, J. Chem. Phys. **53**, 3293 (1970).
[15] V. L. Landau and E. Teller, Phys. Z. Sowjetunion **10**, 34 (1936).
[16] G. Gerber, K. Sakurai, and H. P. Broida, J. Chem. Phys. **64**, 3410 (1976).
[17] C. D. Holmberg, G. S. Williams, and G. P. Perram, J. Chem. Phys. **102**, 6481 (1995).
[18] J. I. Steinfeld, J. Chem. Phys. **46**, 4550 (1967).
[19] J. T. Yardley, *Introduction to Molecular Energy Transfer* (Academic, New York, 1980).
[20] J. Keck and G. Carrier, J. Chem. Phys. **43**, 2284 (1965).
[21] D. Rapp and T. E. Sharp, J. Chem. Phys. **38**, 2641 (1963).
[22] G. P. Perram, D. W. Melton, T. L. Thompson, and W. B. Roh, J. Chem. Phys. **97**, 3258 (1992).